

Design and Implementation of a Si₃N₄ Three-Stigmatic-Point Arrayed Waveguide Grating with a Resolving Power over 17,000

JIAHAO ZHAN,¹ YANG ZHANG,¹ WEI-LUN HSU,¹ SYLVAIN VEILLEUX,² MARIO DAGENAIS^{1,*}

¹Department of Electrical and Computer Engineering, University of Maryland, College Park, MD 20770

²Department of Astronomy, University of Maryland, College Park, MD 20770

*dage@umd.edu

Abstract: To provide a solution to the issue of the non-flat focal surface in traditional Rowland AWGs, we have designed and implemented a Si₃N₄ three-stigmatic-point arrayed waveguide grating (TSP AWG) with a spectral resolving power over 17,000. The flat focal surface of this AWG can accommodate a butt-coupled detector array positioned at the output facet without any reduction of the resolving power of the edge channels. Therefore, it is particularly advantageous to some astronomical applications which require an AWG as a light-dispersing component to obtain a complete 2D spectrum. In addition, because the device is implemented on a high-index-contrast platform (Si₃N₄/SiO₂), a compact dimension of $\sim 9.3 \times 9.3 \text{ mm}^2$ is achieved.

© 2022 Optica Publishing Group under the terms of the [Optica Publishing Group Publishing Agreement](#)

1. Introduction

The novel field of astrophotonics refers to the application of versatile photonic technologies to manipulate guided light collected from telescopes to achieve scientific goals in astronomy [1, 2]. It is widely believed to be a promising approach for solving some major challenges in observational astronomy, one of which is the miniaturization of the next-generation astronomical instrumentation [3]. Astronomers are building larger and larger telescopes, and in fact the next decade will mark the deployment of extremely-large telescopes (ELTs) with diameters (D) over 30 m [4]. As the size and cost of the associated conventional optical setups grow as $D^2 - D^3$, it will become much more challenging to maintain the stability of these giant optical systems. The key idea of astrophotonics is to collapse the bulk optics into 2D photonic integrated circuits to leverage the low-cost, compact, and robust nature of the integrated photonic platform [5–7].

One of the major scientific goals of the ELTs is to study the galaxies in the first billion years of the universe, which requires deep observations of faint sources and extract spectral information from the collected light. For this purpose, an integrated photonic spectrograph (IPS) has been proposed [8], which includes an arrayed waveguide grating (AWG) as the light-dispersing component. AWGs are widely used in modern telecommunication systems as multiplexers and signal routers [9]. As their main functionality is to spatially separate different wavelengths, they are well-suited for spectroscopic applications. The very first on-sky testing with an IPS obtained a spectrum of a type-S star which clearly captured the carbon monoxide molecular absorption features in the H band [10], and successfully demonstrated the possibility of obtaining meaningful astronomical spectra with an AWG.

However, each output channel of an AWG contains periodic pass frequencies from different spectral orders, spaced by the free spectral range (FSR). For astrophotonic spectroscopy applications, a complete spectrum is required and therefore, the overlapping spectral orders in each channel need to be separated by a secondary dispersion setup [11, 12]. A free space cross disperser (e.g. a prism) is often employed to disperse the light in the perpendicular direction, and it is necessary to have the chip cleaved along the output focal plane of the AWG. However, this

45 imposes a challenge on the traditional Rowland AWGs in which the focal surface is a circle. If the
 46 chip is cleaved along the tangent of the Rowland circle [Fig. 1(a)], the offset between the focal
 47 point and the cleaved facet will give rise to defocus aberrations for all channels except for the
 48 central one [Fig. 1(b)]. Thus, a flat focal plane is desired to minimize these defocus aberrations.

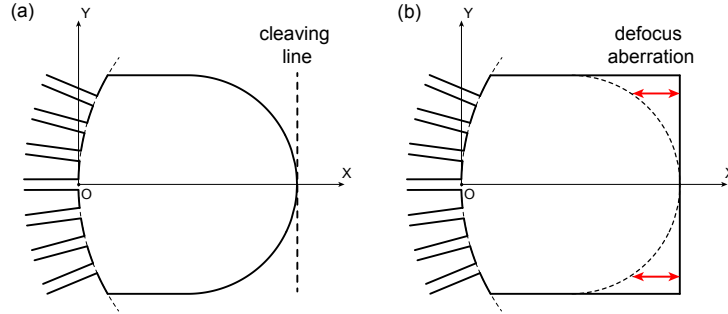


Fig. 1. (a) Mismatch between the circular focal plane and the straight cleaving line. (b) Defocus aberration induced by cleaving. The AWG with a rectangle output star coupler is referred to as a flat-Rowland AWG.

49 One solution is to incorporate a field-flattening lens on top of the output star coupler [13],
 50 which images the circular focal field into a flat one. However, this extra lens layer adds to the
 51 fabrication complexity significantly. Here we present a design and implementation of a Si_3N_4
 52 three-stigmatic-point AWG (TSP AWG) based on the aberration theory proposed in [14, 15].
 53 Different channels of a TSP AWG will inherently be focused onto a flat surface, and there is
 54 no reduction of the resolving power for the edge channels when the device is cleaved along the
 55 focal surface. The measured transmission spectrum of an implemented device shows a spectral
 56 resolving power of over 17,000. Note that when our TSP AWG was under development, A. Stoll
 57 et al. published their results of a similar device on a silica-on-silicon material platform [16]. In
 58 this work, however, not only will we work on a different material platform with a much larger
 59 index contrast ($\text{Si}_3\text{N}_4/\text{SiO}_2$), but we will also provide more details on the design and simulation
 60 processes of the TSP AWG. In addition, we will demonstrate the results of a few-input TSP AWG
 61 which is needed for our future work on the integrated spectrograph topic.

62 2. Theory and Design

63 2.1. Brief summary of the aberration theory

64 A detailed description of the aberration theory is given in [14], and here we provide only a brief
 65 summary. Fig. 2 is a schematic illustration of an AWG, and its structure can be determined by
 66 three functions of w (which corresponds to the Y coordinate in Fig. 2): (1) the shape of the
 67 grating curve $u(w)$, (2) the length of the array waveguides $L(w)$, and (3) the distribution of the
 68 array waveguides along the grating curve $G(w)$. An optical path function (OPF) is defined to
 69 calculate the total path length from the input to one of the output channels:

$$F(w) = n_s [r_A(w) + r_B(w)] + n_w L(w) - G(w)m\lambda \quad (1)$$

70 where n_s and n_w are the effective indices of the star coupler and the array waveguide, m is the
 71 spectral order, $r_A(w)$ [$r_B(w)$] is the geometric length between the input (output) channel and
 72 one of the array waveguides which includes the grating curve function $u(w)$. Note that $G(w)$
 73 does not exist in real optical paths, but it is added such that the OPF is a constant for different
 74 values of w in an aberration-free system.

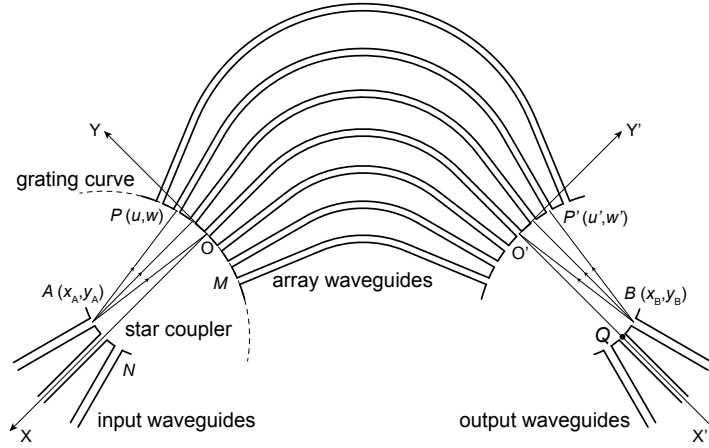


Fig. 2. Schematic illustration of an AWG consisting of I/O waveguides, input and output star couplers (FPRs) and an array of waveguides of different lengths.

75 The OPF can also be expanded into a Taylor series

$$F(w) = F(0) + F'(0)w + \frac{1}{2}F''(0)w^2 + \dots + \frac{1}{n!}F^{(n)}(0)w^n + \dots \quad (2)$$

76 where

$$F^{(n)}(0) = n_s \left[r_A^{(n)}(0) + r_B^{(n)}(0) \right] + n_w L^{(n)}(0) - G^{(n)}(0)m\lambda \quad (3)$$

77 is the n^{th} aberration coefficient. $F^{(2)}(0)$, $F^{(3)}(0)$ and $F^{(4)}(0)$ correspond to the defocus, coma
78 and spherical aberrations, respectively.

79 The key idea to flatten the circular focal surface of a Rowland AWG is to pick a series of
80 collinear "stigmatic" points to define the flat focal surface. The fact that three functions can
81 determine the structure of an AWG dictates that only three points S_i ($i = 1, 2, 3$) can be included.
82 By definition, all aberration coefficients vanish at these stigmatic points. Therefore, with Eq. (3)
83 and the pre-chosen coordinates (x_i, y_i) and wavelengths (λ_i) of the stigmatic points, we have

$$n_s \left[r_A^{(n)}(0) + r_i^{(n)}(0) \right] + n_w L^{(n)}(0) - G^{(n)}(0)m\lambda_i = 0 \quad (4)$$

84 Eq. (4) can be solved in an iterative manner to extract the Taylor coefficients $u^{(n)}(0)$, $L^{(n)}(0)$,
85 and $G^{(n)}(0)$, and then the structure of the TSP AWG can be determined.

86 2.2. Design of a low resolving power TSP AWG

87 As a proof-of-concept demonstration, we started with a TSP AWG of parameters listed in Table
88 1, targeting a low resolving power. The spectral resolving power, which is defined by $R = \lambda/\Delta\lambda$,
89 is an important figure of merit to look for in the transmission spectrum of an AWG.

90 First, the coordinates of the three stigmatic points are selected as $(R_o, 3d_{io})$, $(R_o, 0)$, and
91 $(R_o, -3d_{io})$, corresponding to channel 3, 6 and 9, where R_o is the star coupler radius of the
92 Rowland AWG with the same parameters as in Table 1. The value of R_o is extracted from
93 our simulation software RSoft Photonics Suite. The wavelengths associated with these three
94 stigmatic points are $1.541 \mu\text{m}$, $1.55 \mu\text{m}$, and $1.559 \mu\text{m}$, respectively.

95 Next, $u(w)$, $L(w)$, and $G(w)$ are determined from Eq. (4). The calculated grating curve $u(w)$
96 and the extra length of the array waveguides $L_{ex}(w)$ are plotted in Fig. 3(a) and (b), respectively.

Table 1. List of parameters of the proof-of-concept design.

Parameter	Explanation	Value
N_{in}	Number of input channels	1
N	Number of output channels	11
M	Number of array waveguides	35
λ_c	Center wavelength	$1.55 \mu\text{m}$
$\Delta\lambda$	Wavelength spacing	3 nm
w	Array waveguide width	$2 \mu\text{m}$
d_{ar}	Array waveguide spacing	$6 \mu\text{m}$
d_{io}	I/O waveguide spacing	$6 \mu\text{m}$
R	Resolving Power	~ 960

97 In Fig. 3(a), the calculated grating curve of the TSP AWG is shown by the blue dots, and the
 98 red curve is the corresponding Rowland circle. $L_{ex}(w)$ is calculated by subtracting the length
 99 of the Rowland AWG array waveguides from the calculated total length of the TSP AWG array
 100 waveguides. Comparing with Rowland AWGs, we notice three major structural differences
 101 for a TSP AWG: (1) The grating curve is no longer a circle and it is defined by a polynomial
 102 function instead. (2) The length difference between adjacent waveguides in the array is no longer
 103 a constant, and an extra length is present. (3) The array waveguides are no longer uniformly
 104 distributed along the grating curve.

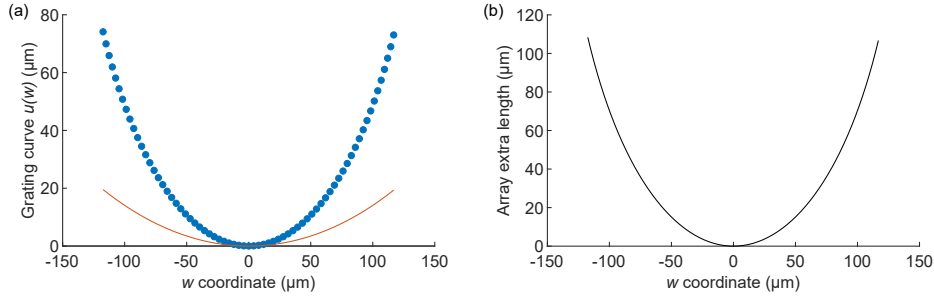


Fig. 3. (a) Calculated grating curve $u(w)$ of the designed TSP AWG (blue dotted), compared to the Rowland circle (red solid). (b) Extra length of the array waveguides of the designed TSP AWG.

105 Finally, the layout design of the TSP AWG must be completed, and the extra length term
 106 $L_{ex}(w)$ needs to be incorporated into the array waveguides. As for Rowland AWGs, it is well
 107 known that the length difference ΔL between adjacent waveguides is given by $\Delta L = m\lambda_c/n_w$.
 108 Each array waveguide comprises three segments: one straight waveguide of length zL_i , one arc
 109 of radius zR_i and angle $2\theta_i$ (in degree), and another straight waveguide identical with the first
 110 one, as depicted in Fig. 4(a). Half of the spacing between the two star couplers is denoted by L_g ,
 111 which determines the minimum bending radius in the array waveguides. R_{end} is the distance
 112 from the input waveguide to the starting point of one of the array waveguides. In the case of a
 113 Rowland AWG, it is a constant equal to the radius of the Rowland circle.

114 Since the length difference between adjacent waveguides is equal to ΔL , the following system
 115 of equations can be derived:

$$\begin{aligned} zR_i \sin \theta_i + (R_{end} + zL_i) \cos \theta_i &= L_g \\ zR_i P \theta_i - zR_1 P \theta_1 + zL_i - zL_1 &= \frac{i-1}{2} \Delta L \end{aligned} \quad (5)$$

116 where $P = \pi/180$. Given the values of ΔL and L_g , Eq. (5) can be solved to obtain zL_i and zR_i ,
 117 and the layout of the array waveguides is determined.

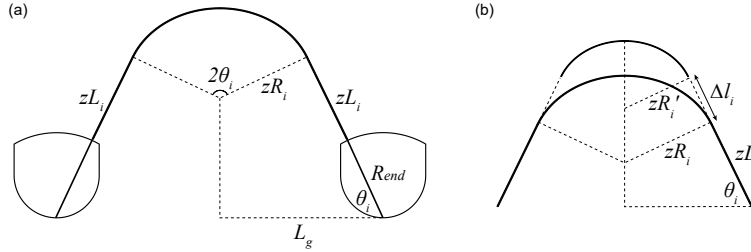


Fig. 4. (a) Array waveguide layout and key parameters in Rowland AWGs. (b) Extending the straight segment to account for the extra length in each array waveguide in TSP AWGs.

118 As for TSP AWGs, there are two main differences: (1) R_{end} is no longer a constant for different
 119 channels, since the star coupler is no longer defined by an arc. (2) There is an extra length
 120 $L_{ex,i}$ associated with each array waveguide. For (1), R_{end} of each channel can be numerically
 121 calculated (denoted by rAr_i), once the grating curve function $u(w)$ is obtained. Fig. 4(b)
 122 demonstrates how the extra length is incorporated in the layout - via the extension of the straight
 123 section with an amount of Δl_i . From some basic geometry, the following system of equations
 124 can be derived:

$$\begin{aligned} L_i &= 2(rAr_i + zL_i + zR_i P \theta_i) \\ L'_i &= 2(rAr_i + zL_i + \Delta l_i + zR'_i P \theta_i) \\ zR'_i &= zR_i - \Delta l_i / \tan \theta_i \\ L'_i - L_i &= L_{ex,i} \end{aligned} \quad (6)$$

125 where L_i and L'_i are the lengths of the array waveguide before and after the extension of the
 126 straight segment, respectively, and the difference between the two is equal to the extra length $L_{ex,i}$.
 127 Solving for Δl_i and zR'_i , the layout of the array waveguides for TSP AWGs can be determined.

128 3. Simulation and experimental results

129 3.1. Device simulation

130 A direct modeling of the TSP AWG in RSoft is difficult, as the built-in AWG simulation utility
 131 supports only the Rowland structures. The general simulation flow in RSoft is: First, a BPM
 132 (Beam-Propagation Method) simulation is performed on the input star coupler, to obtain the
 133 power and initial phase distribution of the array waveguides. Next, the phase is evolved based on
 134 the length of the array waveguides. Then the power and updated phase are combined into an
 135 electric field profile, which will be injected into the output star coupler. Finally the emerging
 136 optical power from the output waveguides are recorded and a complete spectrum can be obtained
 137 by repeating the above steps for all wavelengths.

138 With the same idea in mind, we have developed the following simulation flow for TSP AWGs:
 139 (1) In RSoft, modify the geometry of the input star coupler based on the calculated grating curve
 140 $u(w)$, and perform BPM simulation to obtain initial power and phase information. (2) Modify the
 141 output star coupler similarly, and add launch fields for each array waveguide. Optical modes will
 142 be launched into the output star coupler via these launch fields, and the output power from each
 143 channel will be monitored. (3) Use a custom-developed routine to calculate the phase based on
 144 the length of the array waveguides and create launch field data files for each wavelength. The
 145 entire simulation process is also controlled by this routine.

146 The simulated transmission spectra of the designed TSP AWG with parameters listed in Table
 147 1 and the corresponding Rowland AWG are plotted in Fig. 5(a) and (c), respectively. Fig. 5(b)
 148 and (d) are the calculated resolving powers of the two AWGs with error bars included. The
 149 uncertainty comes from the inaccuracy in the measured 3-dB width of each channel because of
 150 the chosen wavelength step during spectrum simulation, as a compromise for reduced simulation
 151 time. Since N discrete waveguides are placed on the output focal surface to guide the N output
 152 channels, theoretically a well-designed TSP AWG should demonstrate a similar spectral resolving
 153 power compared to the corresponding Rowland AWG. And this is indeed the case comparing Fig.
 154 5(b) and 5(d), which implies that the circular focal surface has been flattened in the TSP AWG.

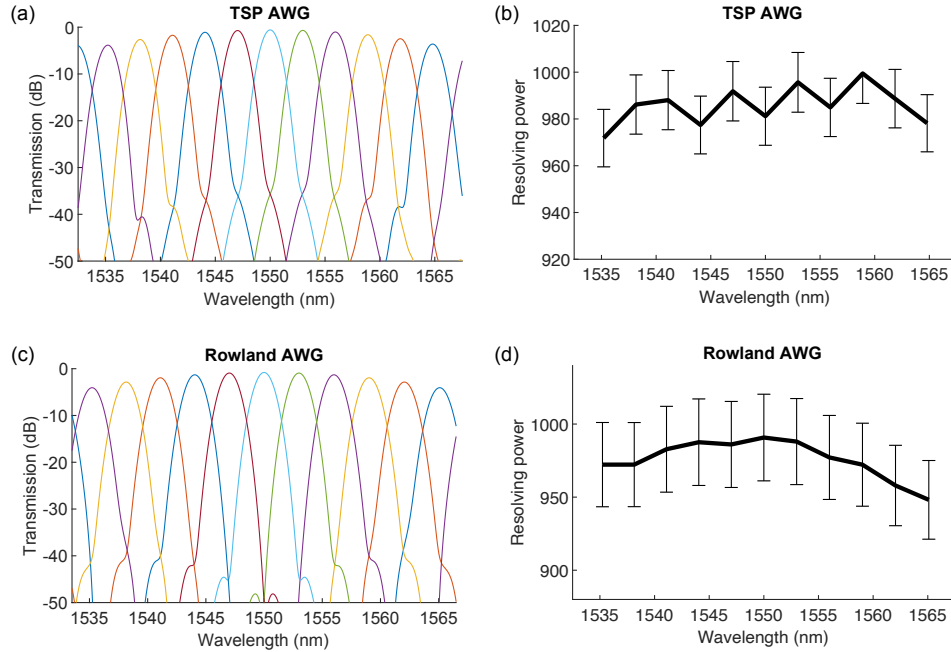


Fig. 5. (a) Simulated transmission spectra and (b) resolving power of the designed TSP AWG. (c) Simulated transmission spectra and (d) resolving power of the corresponding Rowland AWG, with error bars included.

155 3.2. Device fabrication and characterization

156 To better compare the device performances, both the designed TSP AWG and the corresponding
 157 Rowland AWG are fabricated with the following procedures. First, a thin layer (100 nm) of
 158 stoichiometric Si_3N_4 is deposited via low-pressure chemical vapor deposition (LPCVD) on
 159 a silicon wafer with 10- μm thermal SiO_2 on top. Device patterning is performed by e-beam
 160 lithography followed by a developing process to remove the exposed resist. Next, chromium (~

161 20 nm) is deposited as a hard mask, and then the patterns are transferred into the Si_3N_4 layer by
 162 a CHF_3/O_2 -based plasma etching process. After the removal of the Cr hard mask, a top SiO_2
 163 cladding layer is deposited via plasma-enhanced chemical vapor deposition (PECVD). Optical
 164 microscope images of the fabricated Rowland and TSP AWGs are shown in Fig. 6, in which the
 165 structural differences between the two star couplers are clearly demonstrated: the grating curve
 166 of the TSP AWG has a larger curvature, and the focal surface is flat.

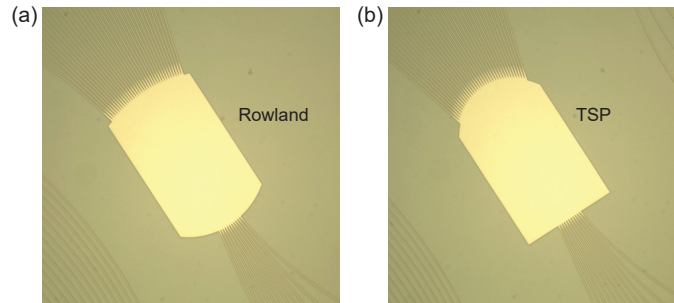


Fig. 6. Optical microscope images of the output star couplers of (a) the Rowland AWG and (b) the TSP AWG. The light enters from the array waveguides at the top, and exits from the output channel waveguides at the bottom.

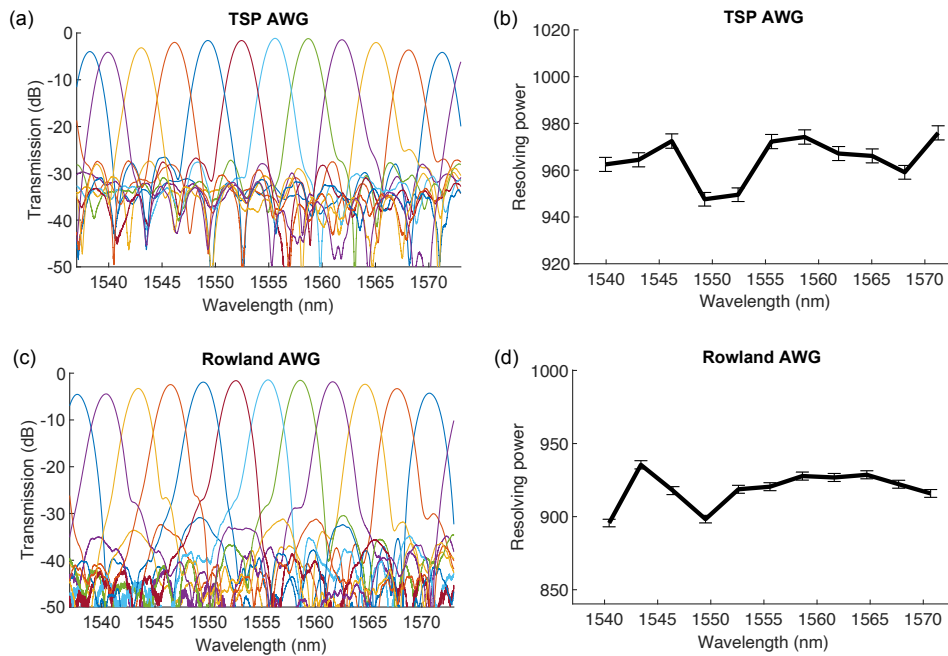


Fig. 7. (a) Measured transmission spectra and (b) calculated resolving power of the designed TSP AWG. (c) Measured transmission spectra and (d) calculated resolving power of the corresponding Rowland AWG, with error bars included.

167 The measured transmission spectra of the fabricated AWGs and the corresponding spectral
 168 resolving power are plotted in Fig. 7. Note that the error bars are much less than those in Fig.
 169 6, since the wavelength sweep was performed with a finer resolution. For both AWGs, a good

170 agreement between the experimental and simulation results is achieved. The throughput of the
 171 fabricated devices is ~ -1.5 dB for the center channel, the side lobes are more than 25 dB down,
 172 and the resolving power is similar to that in the simulation.

173 4. Demonstration of a TSP AWG with a large resolving power

174 For practical applications such as astronomical spectroscopy, TSP AWGs with larger resolving
 175 powers must be implemented. As the above proof-of-concept design works as expected, the same
 176 structure and layout design procedures can be applied. We have designed another TSP AWG
 177 with parameters listed in Table 2. Other parameters not listed are the same as in Table 1. The
 178 dimension of this designed TSP AWG is $\sim 9.3 \times 9.3$ mm², excluding the I/O waveguides.

Table 2. List of parameters of the other two TSP AWGs with higher resolving powers.

Parameter	N_{in}	N	M	$\Delta\lambda$ (nm)	R
Value	3	101	201	0.15	$\sim 17,000$

179 In this case, more than one input channels are included, which is to accommodate multiple
 180 single-mode fibers coming into the AWG. This is a nice-to-have feature for the integrated
 181 spectrograph application, in which the light at the telescope focal plane is first coupled into a
 182 multi-mode fiber, then a so-called “photonic lantern” device [17] adiabatically converts the
 183 multi-mode core into several single-mode cores. The complete layout of this design and optical
 184 microscope images of the fabricated device are provided in the supplemental document.

185 Fig. 8 shows the measurement results of the fabricated device. (a), (c), and (e) correspond to
 186 the transmission spectra measured with the center input channel and the two edge input channels,
 187 respectively. Note that for clarity, only 21 output channels (1 in 5) are plotted in the spectra.
 188 However, the resolving power plots (b), (d), and (f) have all output channels included. The
 189 complete transmission spectra for all three input channels are provided in the supplemental
 190 document. From Fig. 8, it is shown that the throughput of the fabricated device is ~ -2 dB for
 191 the center channel, the side lobes are ~ 15 dB down, and the noise floor is slightly higher than the
 192 results in Fig. 7. To calculate the resolving power of each channel, the 3-dB width is extracted
 193 by finding the two adjacent data points on each side of the peak, and then performing a linear
 194 interpolation. A resolving power of over 17,000 is achieved for all three input channels.

195 5. Conclusion and Outlook

196 We have presented the design and implementation of a Si₃N₄ three-stigmatic-point AWG, with a
 197 detailed discussion of the layout design and simulation method. A spectral resolving power of
 198 over 17,000 has been achieved experimentally. Thanks to the flat focal surface of the TSP AWG,
 199 the defocus aberration of the edge channels is minimized, thus improving the resolving power at
 200 the same time. This design provides a solution for a flat-focal-field spectrometer, fulfilling the
 201 requirement of an integrated astronomical spectrograph in which the chip needs to be cleaved
 202 along the output focal surface to accommodate a linear detector array.

203 As we have mentioned in the last section, a “few-input” AWG is desired in astronomical
 204 spectroscopy applications to interface with a photonic lantern. Another important consideration
 205 is the polarization diversity, as light collected from the universe is unpolarized in nature. It will
 206 be highly advantageous if the integrated photonic spectrograph can handle both polarizations,
 207 when the number of available photons are already quite limited. A polarization-independent
 208 Rowland AWG has been demonstrated by having two inputs for the two polarizations [18]. For
 209 TSP AWGs, a possible solution for including polarization diversity is to first separate the two

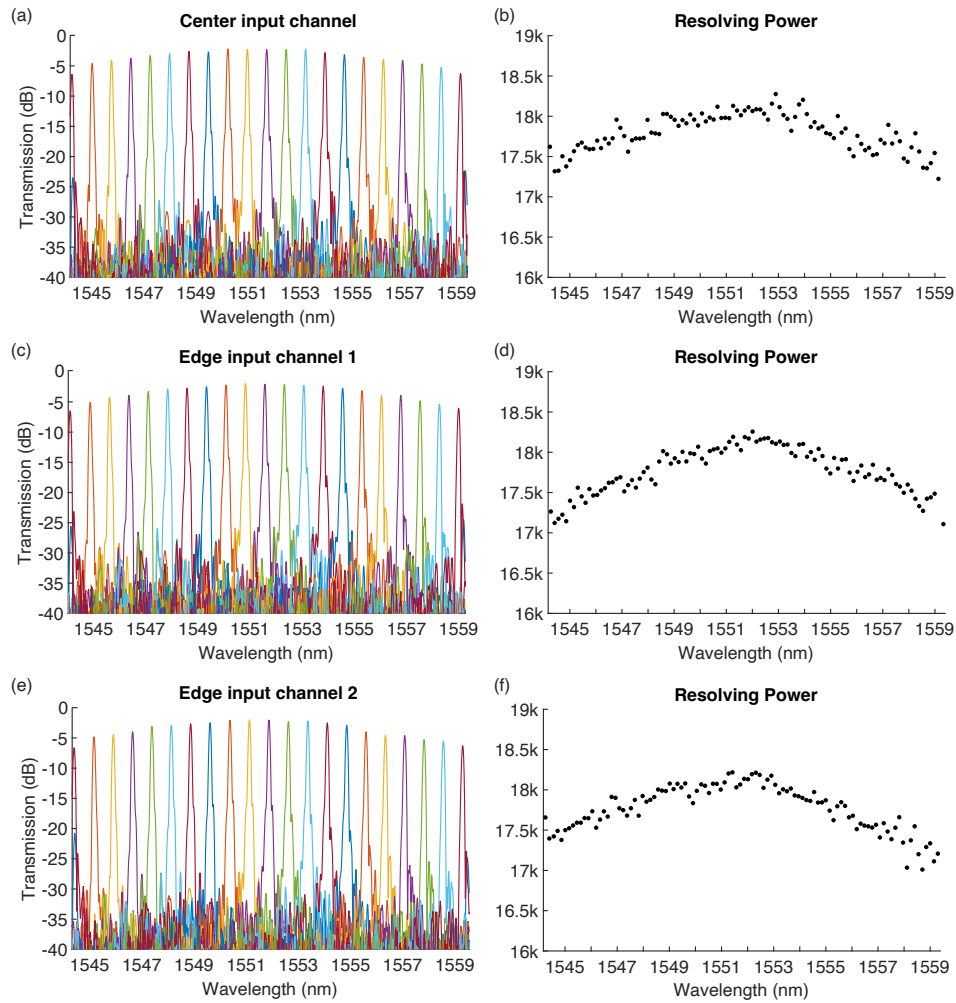


Fig. 8. (a) Measured transmission spectra and (b) calculated resolving power of the large-R TSP AWG, with the input light from the center channel. (c) Measured transmission spectra and (d) calculated resolving power of the large-R TSP AWG, with the input light from one of the edge channels. (e) Measured transmission spectra and (f) calculated resolving power of the large-R TSP AWG, with the input light from the other edge channel. For clarity, only a total of 21 channels are plotted in the transmission spectra. The resolving power plots have all channels included.

210 polarizations with a large-bandwidth polarization beam splitter [19], and then handle the two
 211 polarizations with two customized TSP AWGs.

212 **Funding.** National Science Foundation (NSF) under grant 1711377 and the National Aeronautics and
 213 Space Administration (NASA) under grant 16-APRA 16-0064.

214 **Acknowledgments.** The authors thank Dr. Yi-Wen Hu for the initial development of the MATLAB routine
 215 for the demonstration of the aberration theory, and Dr. Pradip Gatikine for the helpful discussions.

216 **Disclosures.** The authors declare no conflicts of interest.

217 **Data Availability.** Data underlying the results presented in this paper are not publicly available at this
 218 time but may be obtained from the authors upon reasonable request.

219 **Supplemental document.** See Supplement 1 for supporting content.

220 **References**

- 221 1. N. K. Pervez, W. Cheng, Z. Jia, M. P. Cox, H. M. Edrees, and I. Kymissis, "Photonic crystal spectrometer," *Opt.*
222 *Express* **18**, 8277–8285 (2010).
- 223 2. G. Roelkens, U. Dave, A. Gassenq, N. Hattasan, C. Hu, B. Kuyken, F. Leo, A. Malik, M. Muneeb, E. Ryckeboer,
224 S. Uvin, Z. Hens, R. Baets, Y. Shimura, F. Gencarelli, B. Vincent, R. Loo, J. V. Campenhout, L. Cerutti, J.-B.
225 Rodriguez, E. Tournié, X. Chen, M. Nedeljkovic, G. Mashanovich, L. Shen, N. Healy, A. C. Peacock, X. Liu,
226 R. Osgood, and W. Green, "Silicon-based heterogeneous photonic integrated circuits for the mid-infrared," *Opt.*
227 *Mater. Express* **3**, 1523–1536 (2013).
- 228 3. R. J. Harris and J. R. Allington-Smith, "Applications of integrated photonic spectrographs in astronomy," *Mon.*
229 *Notices Royal Astron. Soc.* **428**, 3139–3150 (2012).
- 230 4. J. Bland-Hawthorn and P. Kern, "Astrophotonics: a new era for astronomical instruments," *Opt. Express* **17**,
231 1880–1884 (2009).
- 232 5. K. Chaganti, I. Salakhutdinov, I. Avrutsky, and G. W. Auner, "A simple miniature optical spectrometer with a planar
233 waveguide grating coupler in combination with a plano-convex lens," *Opt. Express* **14**, 4064–4072 (2006).
- 234 6. J. Allington-Smith and J. Bland-Hawthorn, "Astrophotonic spectroscopy: defining the potential advantage," *Mon.*
235 *Notices Royal Astron. Soc.* **404**, 232–238 (2010).
- 236 7. A. Z. Subramanian, E. Ryckeboer, A. Dhakal, F. Peyskens, A. Malik, B. Kuyken, H. Zhao, S. Pathak, A. Ruocco,
237 A. D. Groote, P. Wuytens, D. Martens, F. Leo, W. Xie, U. D. Dave, M. Muneeb, P. V. Dorpe, J. V. Campenhout,
238 W. Bogaerts, P. Bienstman, N. L. Thomas, D. V. Thourhout, Z. Hens, G. Roelkens, and R. Baets, "Silicon and silicon
239 nitride photonic circuits for spectroscopic sensing on-a-chip [invited]," *Photon. Res.* **3**, B47–B59 (2015).
- 240 8. P. Gatkine, S. Veilleux, and M. Dagenais, "Astrophotonic spectrographs," *Appl. Sci.* **9** (2019).
- 241 9. S. Pathak, P. Dumon, D. Van Thourhout, and W. Bogaerts, "Comparison of AWGs and Echelle gratings for wavelength
242 division multiplexing on silicon-on-insulator," *IEEE Photonics J.* **6**, 1–9 (2014).
- 243 10. Cvetojevic, N., Jovanovic, N., Better, C., Lawrence, J. S., Ellis, S. C., Robertson, G., and Bland-Hawthorn, J., "First
244 starlight spectrum captured using an integrated photonic micro-spectrograph," *AA* **544**, L1 (2012).
- 245 11. R. G. Tull, P. J. MacQueen, C. Sneden, and D. L. Lambert, "The high-resolution cross-dispersed Echelle white-pupil
246 spectrometer of the McDonald Observatory 2.7-m telescope," *Publ. Astron. Soc. Pac.* **107**, 251 (1995).
- 247 12. Y.-W. Hu, "Ultra-low-loss silicon nitride waveguide gratings and their applications in astrophotonics," Ph.D. thesis,
248 University of Maryland, College Park (2020).
- 249 13. B. I. Akca, G. Sengo, M. Pollnau, A. Driessen, K. Wörhoff, and R. M. de Ridder, "Flat-focal-field integrated
250 spectrometer using a field-flattening lens," *Opt. Lett.* **37**, 4281–4283 (2012).
- 251 14. D. Wang, G. Jin, Y. Yan, and M. Wu, "Aberration theory of arrayed waveguide grating," *J. Light. Technol.* **19**,
252 279–284 (2001).
- 253 15. S. Lu, C. Yang, Y. Yan, G. Jin, Z. Zhou, W. H. Wong, and E. Y. B. Pun, "Design and fabrication of a polymeric flat
254 focal field arrayed waveguide grating," *Opt. Express* **13**, 9982–9994 (2005).
- 255 16. A. Stoll, K. Madhav, and M. Roth, "Design, simulation and characterization of integrated photonic spectrographs for
256 astronomy II: low-aberration generation-II AWG devices with three stigmatic points," *Opt. Express* **29**, 36226–36241
257 (2021).
- 258 17. S. G. Leon-Saval, A. Argyros, and J. Bland-Hawthorn, "Photonic lanterns: a study of light propagation in multimode
259 to single-mode converters," *Opt. Express* **18**, 8430–8439 (2010).
- 260 18. Q. Han, J. St-Yves, Y. Chen, M. Ménard, and W. Shi, "Polarization-insensitive silicon nitride arrayed waveguide
261 grating," *Opt. Lett.* **44**, 3976–3979 (2019).
- 262 19. J. Zhan, M. Dagenais, G. Yang, and S. Veilleux, "A broadband Si₃N₄ polarization beam splitter based on asymmetric
263 directional couplers," in *2021 Photonics North (PN)*, (2021), pp. 1–1.